Replica exchange Monte Carlo applied to hard spheres

Gerardo Odriozola[a)]
Programa de Ingeniería Molecular, Instituto Mexicano del Petróleo, Lázaro Cárdenas 152, 07730 Mexico, D. F., Mexico

(Received 6 July 2009; accepted 16 September 2009; published online 14 October 2009)

In this work a replica exchange Monte Carlo scheme which considers an extended isobaric-isothermal ensemble with respect to pressure is applied to study hard spheres (HSs). The idea behind the proposal is expanding volume instead of increasing temperature to let crowded systems characterized by dominant repulsive interactions to unblock, and so, to produce sampling from disjoint configurations. The method produces, in a single parallel run, the complete HS equation of state. Thus, the first order fluid-solid transition is captured. The obtained results well agree with previous calculations. This approach seems particularly useful to treat purely entropy-driven systems such as hard body and nonadditive hard mixtures, where temperature plays a trivial role. © *2009 American Institute of Physics*. [doi:10.1063/1.3244562]

I. INTRODUCTION

The replica exchange Monte Carlo (REMC) method,[1,2] also called parallel tempering,[3] was derived to achieve good sampling of systems that present a free energy landscape with many local minima.[4,5] It consists on simulating several replicas of the same system at different thermodynamic states, and allowing for replica exchanges (swap moves). Thus, it is possible to implement an ergodic walk through free energy barriers connecting disjoint configuration subspaces by defining a set of close enough thermodynamic states. Although it has been developed at the end of the last century,[1,2] its acceptance is already high due to its clearness, simplicity, and its wide applicability. Proof of that is its employment to find zeolite structures,[6] to study different conformations of proteins,[7] and to access phase equilibrium of many single and multicomponent systems.[8–10]

Most frequently, the REMC technique is employed to sample an extended canonical ensemble in temperature. Hence, those replicas having larger temperatures are capable of escaping from local free energy minima, where the pair potential attraction of the constituting particles plays a key role. When the free energy minima are mainly dictated by the entropic term, i.e., by the excluded volume repulsive interactions,[11–13] enlarging the temperature has a small effect. In other words, the benefits of the method become restricted. This is especially true when dealing with hard body systems (purely entropy-driven systems) such as hard spheres (HSs), rods, plates, polymers, and nonadditive hard mixtures, since they constitute limiting cases where the pair interactions are repulsive only and the temperature plays a trivial (null) role. Thus, it is not very surprising that the REMC technique has not been applied yet to this kind of systems. To do this, an alternative would be performing the ensemble extension in pressure instead of temperature, to provide the particles more freedom to rearrange as the volume expands. This idea is tested in this work for HS.

[a)]Electronic mail: godriozo@imp.mx.

It is well known that fluid-solid transitions represent a challenge for computational science.[14,15] Most techniques which properly work for accessing liquid-gas transitions have problems at very high densities.[5] Therefore, the freezing and melting points are at least difficult to determine.[14] Indeed, for the HS model, simulations have recently produced an accurate determination of the freezing and melting point theoretically reported in the sixties.[14,15] That is despite the intense study of HS through the past decades, and the fact that the HS model was one of the first systems ever studied by computer simulations.[16–18] Additionally, the HS model shows a high density metastable branch ending at the random close package density,[19] which adds difficulty for sampling from equilibrium.

The aim of this study is to show that the REMC can be successfully applied to study hard body systems. Hence, the REMC is used by performing a NPT ensemble extension on pressure and applied to HS. The paper is structured as follows. Section II describes the employed algorithm. Results are given in Sec. III. Finally, in Sec. IV conclusions are drawn.

II. NUMERICAL METHOD

As mentioned, in the parallel tempering scheme n_r identical replicas are considered, each following a typical canonical simulation. However, a different temperature is set for each one of them. Thus, an extended ensemble can be defined so that its partition function is $Q_{\text{extended}}=\Pi_{i=1}^{n_r} Q_{NVTi}$, being Q_{NVTi} the partition function of ensemble i at temperature T_i, number of particles N, and volume V. The existence of this extended ensemble justifies the introduction of swap trial moves between any two ensembles (each ensemble is sampled by only one replica at a time), whenever the detail balance condition is satisfied. If all $(i,T_i)(j,T_j) \rightarrow (j,T_i)(i,T_j)$ swap trials have the same *a priori* probability of being performed, the swap acceptance probability becomes

 © 2009 American Institute of Physics

Downloaded 11 Feb 2010 to 128.119.50.56. Redistribution subject to AIP license or copyright; see http://jcp.aip.org/jcp/copyright.jsp

$$P_{\text{acc}} = \min\{1, \exp[(\beta_j - \beta_i)(U_i - U_j)]\}, \quad (1)$$

where $\beta_i = 1/(k_B T_i)$ is the reciprocal temperature of replica i, k_B is Boltzmann's constant, and U_i is the energy of replica i. Hence, by introducing these swap trials, a particular replica seals through many temperatures allowing it to overcome free energy barriers. Additionally, sampling on particular ensembles is not disturbed but enriched by the different contributions of the n_r replicas.

For studying systems where excluded volume interactions dominate, it may be convenient to allow the replicas to expand for destroying any local order. Additionally, in the case of a HS system (or any other purely entropy-driven model) an extended ensemble in temperature is pointless, since this variable does not affect the system structure. For that purpose, the extended ensemble is defined as $Q_{\text{extended}} = \prod_{i=1}^{n_r} Q_{NTPi}$, being Q_{NTPi} the partition function of the isobaric-isothermal ensemble of system i, at pressure P_i, fixed temperature T, and number of particles N (note that the extension is in pressure; an isobaric-isothermal extension in temperature applied to a Lennard-Jones system is given by Okabe *et al.*[20]). This extended ensemble can be sampled by performing standard NTP simulations on each replica, which implies typical particle displacement trials and volume change trials. Notwithstanding, the sampling can be significantly improved by introducing swap trials between neighboring ensembles. Again, the only restriction is that the detail balance condition must prevail to guaranty the correct sampling. One way of achieving this is by setting equal all *a priori* probabilities of choosing the different adjacent pairs of replicas, and accounting for the following acceptance probability

$$P_{\text{acc}} = min\{1, \exp[\beta(P_i - P_j)(V_i - V_j)]\}, \quad (2)$$

where $V_i - V_j$ is the volume difference between replicas i and j. It should be noted that the ensemble extension in pressure leads to a simple acceptance rule where energy terms vanish.

For $(P_i - P_j)(V_i - V_j) \geq 0$, $P_{\text{acc}} = 1$ and so, the acceptance rule tends to order the replicas by volume size (lower volumes at higher pressures). For $(P_i - P_j)(V_i - V_j) < 0$, P_{acc} depends on the absolute value of the pressure differences of the adjacent ensembles, $\beta|P_i - P_j|$. A decrease in $\beta|P_i - P_j|$ leads to a larger acceptance probability. Consequently, adjacent pressures should be close enough to provide large exchange acceptance rates between neighboring ensembles. This is particularly important where a phase transition takes place (characterized by large $|V_i - V_j|$), which generally leads to a bottleneck of the swap acceptance rate. Additionally, the swap acceptance rate also depends on the system size. Larger system sizes produce narrower distribution of densities (volumes) for a given pressure, providing smaller overlap regions between adjacent ensembles. Hence, a larger system size leads to a decrease in the swap acceptance probability. Finally, in order to take a good advantage of the method, the replica at the lowest pressure must assure large jumps in configuration space, so that the higher pressure ensembles can be sampled from disjoin configurations.

In this work, $n_r = 70$ cubic boxes of initial side L are considered. These boxes are filled by randomly placing N HSs of diameter σ. The initial density, $\rho = N\pi\sigma^3/(6L)$, is set to 0.30 for all replicas. A geometrically increasing pressure, βP, is set from approximately 2 to $100\sigma^{-3}$, and arbitrarily assigned to the replicas. Where the fluid-solid transition is expected, intermediate pressures are added (the total number of replicas equals the number of different pressures). An optimal allocation of replicas should lead to a constant swap acceptance probability for all pair of adjacent ensembles.[21] Two experiments were done, one with $N = 32$ and the other with $N = 108$. The simulation starts by following the trial moves above described (see the appendix for details).

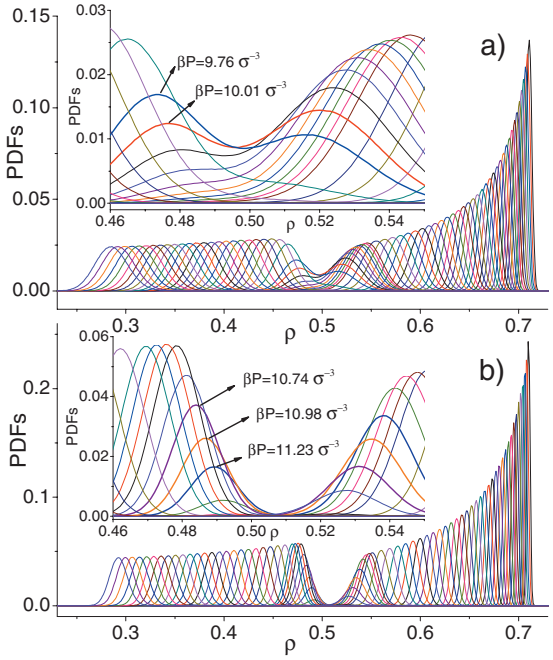

FIG. 1. PDFs to find a replica at a given density, ρ. The 70 different curves correspond to the different assigned pressures. (a) corresponds to $N = 32$ and (b) to $N = 108$. Both insets zoom in the corresponding data.

Sampling consists on measuring densities, radial distribution functions (RDFs), average number of neighbors, and the order parameter Q_6, as a function of the pressure. The average number of neighbors, N_n, is computed accounting for all pairs having a center-center distance smaller than 1.2σ (the vectors joining the centers of these pairs are named bonds). The order parameter Q_6 is defined as[19,22]

$$Q_6 = \left(\frac{4\pi}{13} \sum_{m=-6}^{m=6} |\langle Y_{6m}(\theta, \phi) \rangle|^2 \right)^{1/2}, \quad (3)$$

where $\langle Y_{6m}(\theta, \phi) \rangle$ is the average over all bonds and configurations of the spherical harmonics of the orientation angles θ and ϕ (these are the polar angles of the bonds measured with respect to any fixed coordinate system, since Q_6 is invariant). Q_6 should go to zero for a completely random system of a large number of points, following $1/\sqrt{NN_n/2} \pm 1/\sqrt{13NN_n}$.[19]

III. RESULTS

Figure 1(a) shows the probability density functions (PDFs) to find a replica at a given density for all pressures and for $N = 32$. The 70 PDFs correspond to the different assigned pressures. In general, the PDFs are bell-shaped and

Downloaded 11 Feb 2010 to 128.119.50.56. Redistribution subject to AIP license or copyright; see http://jcp.aip.org/jcp/copyright.jsp

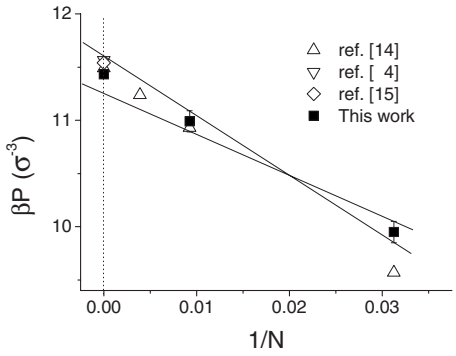

FIG. 2. βP as a function of the inverse of the system size, $1/N$. Solid symbols correspond to this work results. The solid symbol at $1/N=0$ is an extrapolation of the data and the solid lines are drawn to estimate the corresponding error. Open symbols are values reported by different authors.

centered on a maximum which location depends on the assigned pressure. The leftmost curve corresponds to the lowest pressure $(2.16\beta^{-1}\sigma^{-3})$ and the rightmost to the highest one $(100\beta^{-1}\sigma^{-3})$. As pressure increases, the curves narrow and shift to the right producing larger densities (the narrowing is very pronounced for high pressures). The exception occurs for densities close to 0.5, where the PDFs split yielding bimodal distributions. At $\rho \simeq 0.5$, the replicas produce few configurations, and the bimodals yield a local peak below 0.49 and another above 0.51. Thus, a jump on density from $\rho_f=0.474$ to $\rho_s=0.520$ is produced for $\beta P=(9.95\pm0.10)\sigma^{-3}$, pointing out the well-known HS fluid-solid transition. The inset of Fig. 1(a) zooms in the density region around 0.5, where the PDFs are much clearly seen. There it is shown the pressures that correspond to the PDFs which are closer to the transition.

The PDFs obtained for $N=108$ are shown in Fig. 1(b). As expected, similar trends are seen. That is, PDFs are bell-shaped, they narrow and shift toward larger densities for increasing pressure, and they turn bimodal for densities close to 0.5. Nevertheless, PDFs are higher (approximately two times higher) and (consequently) narrower than for $N=32$. Also the bimodal distributions become sharper producing interpeak regions rarely visited by the replicas. In fact, for $\rho \simeq 0.508$ the PDFs are practically zero. In other words, the HS fluid-solid transition turns more evident by increasing the system size. As in Fig. 1(a), the inset of Fig. 1(b) zooms in the corresponding PDFs. From there it can be estimated the transition occurring at $\beta P=(10.99\pm0.10)\sigma^{-3}$ with $\rho_f=0.487$ and $\rho_s=0.538$. Thus, the transition occurs at a higher pressure and shifts to larger densities for increasing the system size. The gap between the fluid and solid densities also enlarges.

The data obtained for small N values can be extrapolated to estimate the HS bulk coexistence pressure, fluid density, and solid density. These are $\beta P_{tr}=(11.43\pm0.17)\sigma^{-3}$, $\rho_f=0.492\pm0.004$, and $\rho_s=0.545\pm0.004$, respectively. These values are in good agreement with previous calculations.[5,14,15] Figure 2 shows the extrapolation for the coexistence pressure, and a comparison with data reported by different authors. As can be seen, the obtained agreement is good, suggesting that the RECM method works properly for capturing the HS fluid-solid transition.

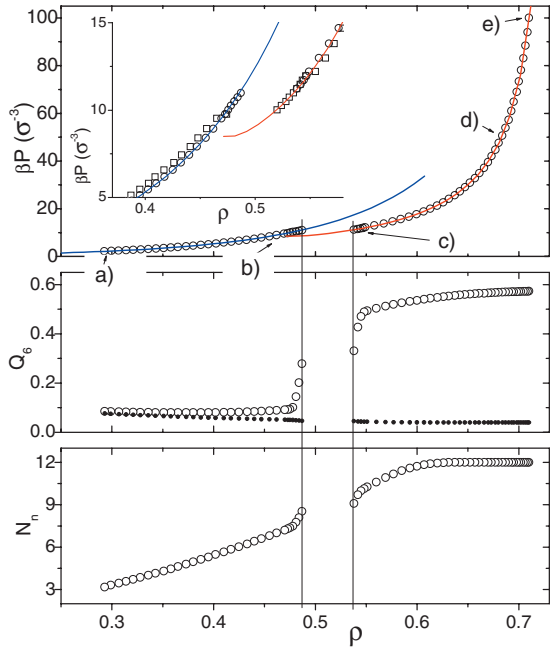

FIG. 3. Topmost: HS equation of state (pressure as a function of the corresponding most frequent density) for $N=108$ (○ symbols). The red line corresponds to the HS fluid equation of state of Speedy (Ref. 23) and the blue one to the HS fcc equation of state of the same author (Ref. 24) Inset: zoom in of the same plot, where □ symbols were added corresponding to $N=32$. Middle plot; Order parameter, Q_6, as a function of ρ (○ symbols), and the corresponding value for a completely random system of points $1/\sqrt{NN_n/2}$ (small bullets). Bottommost; Number of first neighbors, N_n, as a function of ρ.

The topmost plot of Fig. 3 is built by plotting the pressure as a function of the most frequent density for $N=108$. It is also shown as a red line a Padé approximation to data obtained from the HS fluid state,[23] and as a blue line a fit to the HS face cubic centered (fcc) solid state,[24] both data series obtained by means of simulations. As an inset, it is shown a zoom in of the same data for the coexistence, where there were added the data obtained for $N=32$. Both curves here reported, for the fluid and solid states, well agree with the equation of state given by Speedy. This confirms the good behavior of the REMC ensemble extension on pressure. Nevertheless, there is a slight deviation from the fcc curve of Speedy close to the transition. This may signal the presence of hexagonal close-packed (hcp) arrangements and even hybrid fcc-hcp structures.

The middle and bottommost plots of Fig. 3 show the order parameter, Q_6, and the number of first neighbors, N_n, as a function of ρ, respectively. The middle plot also shows as bullets the value of Q_6 for completely space-uncorrelated particles. As expected, Q_6 is small for the fluid region, pointing out the practical absence of angular order. However, it is always somewhat larger than the value of Q_6 for a random system. The difference between these two values diminishes for decreasing ρ. On the other hand, Q_6 reaches 0.5732 for $\beta P=100\sigma^{-3}$, which is slightly lower than the Q_6 value of the fcc arrangement, 0.5745, and well above the corresponding value of the hcp structure, $Q_6=0.4848$. This signals that only replicas approaching the fcc lattice are allowed for the highest applied pressures. This is not surprising since 108 iden-

Downloaded 11 Feb 2010 to 128.119.50.56. Redistribution subject to AIP license or copyright; see http://jcp.aip.org/jcp/copyright.jsp

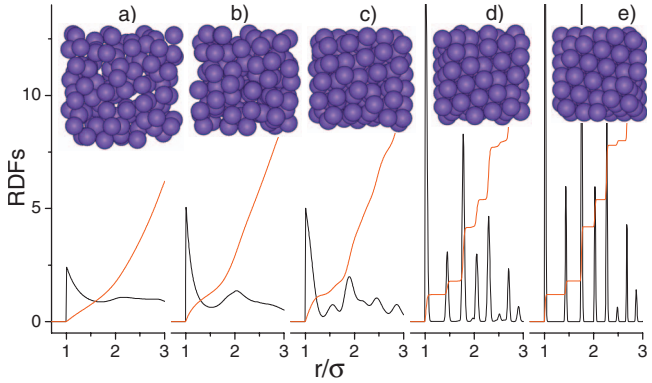

FIG. 4. RDFs (black lines) and their integrals (red lines) for cases (a), (b), (c), (d), and (e), as shown in Fig. 3, from left to right. The insets are the corresponding snapshots. Integrals (red lines) are scaled by a factor 1/10.

tical spherical particles can be perfectly packed on a cubic box on a fcc lattice, but cannot on a hcp lattice. Thus, the system is being forced to promote fcc over hcp at high pressures. For lower but still over the coexistence pressures, Q_6 is close to 0.5, suggesting that both lattices and their hybrids contribute to the average. It should be noted that Q_6 sharply increases at the fluid-solid transition. Thus, it can be employed to detect any trace of local angular order. This was shown to be much more reliable than the RDF peak that develops close to 1.5σ.[19] Finally, N_n monotonically increases with ρ. It also shows a sharp increase at the coexistence, although less pronounced than for Q_6. At large densities N_n reaches 12, which is the largest possible HS coordination number, as it is well known.

The RDFs and their corresponding integrals for cases (a), (b), (c), (d), and (e) pointed out in Fig. 3 are plotted in Fig. 4. Cases (a) and (b) correspond to the fluid phase, and the other three correspond to the solid phase. Case (a) shows the typical low density liquid structure, where a relatively small contact value is developed and the second shell of neighbors is poorly seen. As the density increases, case (b), the RDF shows a larger contact value [two times larger than case (a)], and a well-defined second shell of neighbors. This case corresponds to a liquid close to the coexistence. Slightly above the coexistence, the RDF looks like case (c). Here a small peak appears at $r/\sigma \simeq 1.5$, whereas the valley in-between this peak and the contact one deepens. Other peaks also form at larger distances. For density values close to 0.68, case (d), the RDF develops the full character of a crystal. That is, peaks are very high and narrow, and valleys turn practically zero. The integral (red line) of this case highlights this fact, since it shows a steplike behavior. The first step reaches 12, pointing out the first shell coordination number (integral of the peak at $r/\sigma=1$), the second yields 18 ($r/\sigma=\sqrt{2}$), the third 42 ($r/\sigma=\sqrt{3}$), and the fourth 54 ($r/\sigma=2$), what corresponds to the fcc structure. Nonetheless, a small shoulder appears at the left of the fourth peak ($r/\sigma=\sqrt{11/3} \simeq 1.91$), suggesting the existence of few configurations having a hcp structure. For larger densities, case e), this shoulder disappears and a practically pure fcc RDF is observed.

IV. CONCLUSIONS

This work shows that a REMC scheme can be successfully applied to study HSs at high densities. For that purpose, an extension of the isobaric-isothermal ensemble with respect to pressure is used. The algorithm employs standard particle trial displacements and volume changes together with replica exchanges (swap moves). These easy to implement trials are shown to be enough for capturing the fluid-solid transition of HSs and the solid equilibrium branch for small systems. The obtained results well agree with previous calculations. The principal idea behind this scheme is to increase the particles mobilities by decreasing the pressure (expanding the volume), so that systems characterized by large excluded volume contributions are able to visit disjoint configurations of configurational space. This approach seems particularly useful to deal with purely entropy-driven systems such as hard body and nonadditive hard mixtures, where temperature plays a trivial role.

APPENDIX: SIMULATION DETAILS

Once the $n_r=70$ boxes are filled with the N spheres and are assigned the corresponding different pressures, the algorithm starts performing the trials. As mentioned, they are: particle displacements, volume changes, and swap moves. The probability for selecting a particle displacement trial (in any of the n_r boxes), P_d, is fixed to $P_d=n_rN/[n_r(N+1)+w(n_r-1)]$. The probabilities for selecting a volume change trial, P_v, and a swap trial, P_s, are $P_v=n_r/[n_r(N+1)+w(n_r-1)]$ and $P_s=w(n_r-1)/[n_r(N+1)+w(n_r-1)]$. Here, w is a weight factor fixed to 1/50. Additionally, the probability of performing a particle displacement trial and a volume change trial in a replica enlarges as it is closer to the fluid-solid transition pressure. These probabilities are 10 times larger for the central replica than for those having the highest and the lowest pressures. All particles of a given replica have the same *a priori* probability of being selected to perform a displacement trial. The same is true for selecting a pair of adjacent replicas to attempt a swap move (there are n_r-1 pairs). Thus, a random number homogeneously distributed in [0,1] is generated in order to determine the type of trial to be performed. In case of selecting a particle displacement, the algorithm provides the replica and the particle for applying the trial. In case of a volume change trial, it identifies the replica; and in case of a swap trial, the algorithm gives the adjacent replicas to apply it. Next, another random number is generated to produce a second trial. If these two trials are independent the one another (for instance, they are particle trials on different replicas) the algorithm generates a third trial (note that these trials are not being applied yet). This procedure is repeated until the last trial cannot be performed independently of the others (for instance, a particle displacement trial on a replica in which a volume change trial must be previously performed). This way, the algorithm have randomly selected a given number of independent trials to be applied on the replicas. Immediately after, the algorithm parallelizes (in two threads, since a dual core desktop is used), and the trials are done. The last generated trial (which was not yet performed) becomes now the first trial to be applied on the following series of trials. This procedure is followed to strictly preserve the detail balance condition (to build a symmetric transition matrix) while performing a paralleliza-

Downloaded 11 Feb 2010 to 128.119.50.56. Redistribution subject to AIP license or copyright; see http://jcp.aip.org/jcp/copyright.jsp

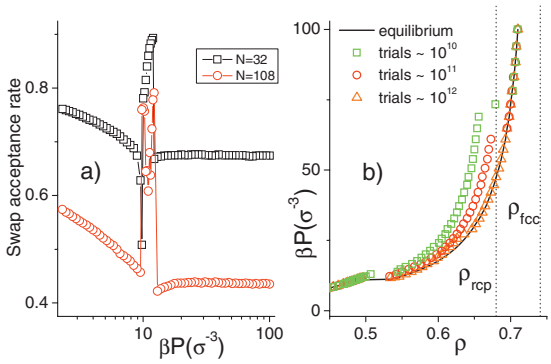

FIG. 5. (a) Swap acceptance rate as a function of the ensemble pressure. (b) Evolution of the densities with the number of trials during the initializing procedure ($N=108$). As a reference, the data obtained from equilibrium are added as a solid line. The dotted lines show the RCP density as obtained from the square symbols and the fcc density.

tion. Verlet lists are employed for saving CPU time (note that the saving can be quite large since replicas at high pressures rarely update their lists).

Sampling is not performed for the first 3.0×10^{12} trials (initializing procedure). During this process, the maximum displacements of particles and maximum volume changes for each pressure are tuned to yield acceptance rates close to 0.4. Thus, particle maximum displacements and maximum volume changes in ensembles having high pressures turn smaller than those associated to ensembles having low pressures. Once this is done, all maximum displacements (one for each pressure) and maximum volume changes (also one for each pressure) become fixed. 1.0×10^{13} trials are then employed to yield the data shown in the body of the article (equilibrium sampling).

The acceptance rates obtained for the swap trials are shown in Fig. 5(a) as a function of the pressure, βP. As expected, the acceptance rates for the smaller system ($N=32$) are, in general, larger than the ones obtained for the larger system ($N=108$). This is a consequence of the larger overlaps of the distributions. In both cases the values are above the recommended acceptance rate of 0.2.[21] For $\beta P > \beta P_{tr}$, the acceptance rate is practically constant. On the contrary, for $\beta P < \beta P_{tr}$, the acceptance rate increases with decreasing βP. This means that for the fluid region, βP should be reduced more than geometrically for optimization purposes. For $10 \lesssim \beta P \lesssim 12$, the acceptance rate increases. This is due to the fact that smaller pressure differences are set between the adjacent ensembles to compensate the natural decrease in the acceptance rate at the fluid-solid transition. Note that more than the necessary replicas are added in order to decrease the error of the coexistence pressure (the natural decrease in the acceptance rate is overcompensated). In addition, this study is focused on yielding a detailed sampling of a large βP range. To acquire equilibrium data from a high pressure system only, many fewer replicas would be required (the optimal swap acceptance rate is close to 20% when temperature is employed as the thermodynamic variable of ensemble extension[21]).

Figure 5(b) shows the evolution of the pressure versus density plot with the number of performed trials during the initializing procedure ($N=108$). For $\sim10^{10}$ trials, the sampling yields a curve at $\beta P > \beta P_{tr}$ which may correspond to the random close packing (RCP) metastable branch. There are also 5 replicas which reached the equilibrium state (since they crystallized, they were pushed toward the highest pressure region). Another one, producing the point lying on the dotted line, may correspond to a partially crystallized structure. Assuming this well-defined curve corresponds to the RCP branch, $\rho_{RCP}=0.680\pm0.005$ is obtained from $\beta P/\rho^2 \propto (\rho_{RCP}-\rho)^{-1}$.[19] This is larger than the reported value of $\rho_{RCP}=0.644\pm0.005$,[19] suggesting that some degree of crystallization is already taking place on the replicas at high pressure. This is in fact confirmed by the Q_6 analysis (not shown). As the initializing process advances, the degree of crystallization augments and the high pressure curve shifts approaching the equilibrium branch (Q_6 also enlarges). For $\sim10^{12}$ trials, the curve practically yields the equilibrium branch. From here on, only those replicas having a large degree of crystallinity are able to access the high pressure region. At this point, the initializing procedure ends and the sampling from equilibrium process starts.

[1] A. P. Lyubartsev, A. A. Martsinovski, S. V. Shevkunov, and P. N. Vorontsov-Velyaminov, J. Chem. Phys. **96**, 1776 (1992).
[2] E. Marinari and G. Parisi, Europhys. Lett. **19**, 451 (1992).
[3] Q. L. Yan and J. J. de Pablo, J. Chem. Phys. **111**, 9509 (1999).
[4] E. Bittner, A. Nußbaumer, and W. Janke, Phys. Rev. Lett. **101**, 130603 (2008).
[5] D. Frenkel and B. Smit, *Understanding Molecular Simulation* (Academic, New York, 1996).
[6] M. Falcioni and M. W. Deem, J. Chem. Phys. **110**, 1754 (1999).
[7] J. Hernández-Rojas and J. M. G. Llorente, Phys. Rev. Lett. **100**, 258104 (2008).
[8] C. E. Fiore, Phys. Rev. E **78**, 041109 (2008).
[9] A. Imperio and L. Reatto, J. Chem. Phys. **124**, 164712 (2006).
[10] A. Arnold and C. Holm, Eur. Phys. J. E **27**, 21 (2008).
[11] A. Fortini and M. Dijkstra, J. Phys.: Condens. Matter **18**, L371 (2006).
[12] G. Odriozola, F. Jiménez-Ángeles, and M. Lozada-Cassou, J. Chem. Phys. **129**, 111101 (2008).
[13] F. Jiménez-Ángeles, Y. Duda, G. Odriozola, and M. Lozada-Cassou, J. Phys. Chem. C **112**, 18028 (2008).
[14] N. B. Wilding and A. D. Bruce, Phys. Rev. Lett. **85**, 5138 (2000).
[15] E. G. Noya, C. Vega, and E. de Miguel, J. Chem. Phys. **128**, 154507 (2008).
[16] M. N. Rosenbluth and A. W. Rosenbluth, J. Chem. Phys. **22**, 881 (1954).
[17] W. W. Wood and J. D. Jacobson, J. Chem. Phys. **27**, 1207 (1957).
[18] B. J. Alder and T. E. Wainwright, J. Chem. Phys. **27**, 1208 (1957).
[19] M. D. Rintoul and S. Torquato, J. Chem. Phys. **105**, 9258 (1996).
[20] T. Okabe, M. Kawata, Y. Okamoto, and M. Mikami, Chem. Phys. Lett. **335**, 435 (2001).
[21] N. Rathore, M. Chopra, and J. J. de Pablo, J. Chem. Phys. **122**, 024111 (2005).
[22] P. J. Steinhardt, D. R. Nelson, and M. Ronchetti, Phys. Rev. B **28**, 784 (1983).
[23] R. J. Speedy, J. Phys.: Condens. Matter **9**, 8591 (1997).
[24] R. J. Speedy, J. Phys.: Condens. Matter **10**, 4387 (1998).

Downloaded 11 Feb 2010 to 128.119.50.56. Redistribution subject to AIP license or copyright; see http://jcp.aip.org/jcp/copyright.jsp